Aus dem Department Biologische Wissenschaften und Pathobiologie
der Veterinärmedizinischen Universität Wien
Zentrum für Pathobiologie
Institut für Pathologie
(Leiter: Univ.-Prof. Dr. med. vet. Herbert Weissenböck Dipl. ECPHM)

Diagnostic Insights in a Case of Canine Primary Central Nervous System Lymphoma

Diplomarbeit

Veterinärmedizinische Universität Wien

vorgelegt von

Lisa-Maria Cs.Tóth

Wien, im Juli 2025

Betreuerin:

Ass.-Prof. Dr. med. vet. Angelika Suchy

Pathologie
Zentrum für Pathobiologie
Department Biologische Wissenschaften und Pathobiologie
Veterinärmedizinische Universität Wien

Gutachterin:

Ass.-Prof. Dr. med. vet. Katharina Hittmair

Bildgebende Diagnostik
Klinisches Zentrum für Kleintiere
Klinisches Department für Kleintiere und Pferde
Veterinärmedizinische Universität Wien

Eigenständigkeitserklärung

Hiermit erkläre ich, dass ich die vorgelegte Arbeit selbstständig verfasst und keine anderen als die angegebenen Quellen und Hilfsmittel benutzt habe. Alle übernommenen Textstellen aus fremden Quellen wurden kenntlich gemacht.
Die vorliegende Arbeit wurde nicht an anderer Stelle eingereicht oder veröffentlicht.

Wien, den 25. Juli 2025

Lisa-Maria Cs.Tóth

Table of Content

Abstract

The case of a 9-year-old neutered male mixed-breed dog with progressive neurological symptoms including altered gait, behaviorial changes, and difficulty swallowing was presented to the Emergency Unit at the University of Veterinary Medicine, Vienna. Due to the clinical findings the patient was initially referred to intensive care for stabilization and further examination, which included a neurologic examination, magnetic resonance imaging of the head, and laboratory tests.

A follow-up neurological examination revealed episodes of nystagmus (alternating from horizontal to torsional), slow pupillary light reflexes and reduced oculocephalic reflexes, anisocoria, and ultimately tetraparesis. Magnetic resonance imaging of the brain was unremarkable; however, cerebrospinal fluid analysis showed distinct cytological features of malignancy with high cellularity and pleomorphic cells. According to these results and the poor prognosis, the owners decided against further treatment and chose euthanasia. As part of the subsequent autopsy, histopathological examination revealed lymphoid infiltration primarily of the meninges, thereby confirming the suspected diagnosis of primary central nervous system lymphoma. Thus, unremarkable magnetic resonance imaging findings do not rule out central nervous system lymphoma and should be validated and supplemented by cerebrospinal fluid analysis.

Zusammenfassung

Präsentiert wird der Fall eines neun Jahre alten, 20 kg schweren, kastrierten Mischlingsrüden, welcher mit einer zweiwöchigen Vorgeschichte von fortschreitenden neurologischen Symptomen, darunter Gangbildstörungen, Wesensveränderung und Schluckbeschwerden in der Zentralen Notaufnahme der Veterinärmedizinischen Universität Wien vorstellig wurde. Aufgrund der ersten klinischen Befunde wurde der Patient zur Stabilisierung und weiterführenden Diagnostik auf die Intensivstation überwiesen. Im Zuge der neurologischen Untersuchung zeigten sich Episoden von wechselndem Nystagmus, verlangsamte Pupillenlichtreflexe und letztendlich eine Tetraparese. Obwohl die Aufnahmen der Magnetresonanztomographie des Kraniums unauffällig waren, zeigte die zytologische Untersuchung des Liquors mit einer deutlich erhöhten Zellzahl und einem insgesamt pleomorphem Zellbild eindeutige Merkmale eines malignen Prozesses. Die Besitzer

entschieden sich aufgrund dieser Ergebnisse und der damit verbundenen schlechten Prognose gegen einen Therapieversuch und für eine Euthanasie. Im Rahmen der nachfolgenden Autopsie erbrachte die pathohistologische Untersuchung eine vornehmlich meningeale, diffuse lymphoidzellige Infiltration und bestätigte damit die Verdachtsdiagnose eines primären Lymphoms des zentralen Nervensystems. Unauffällige Magnetresonanztomographie-Befunde schließen somit die Diagnose eines Lymphoms des zentralen Nervensystems nicht aus und sollten daher zumindest durch die Analyse der Cerebrospinalflüssigkeit ergänzt werden.

List of abbreviations

ADC	Apparent diffusion coefficient
CBC	Complete blood count
CNS	Central nervous system
CNSL	Central nervous system lymphoma
CSF	Cerebrospinal fluid
CT	Computer tomography
DLBCL	Diffuse large B-cell lymphoma
DWI	Diffusion-weighted imaging
GME	Granulomatous meningoencephalitis
HE	Hematoxylin and eosin
HL	Hodgkin Lymphoma
ICU	Intensive care unit
IHC	Immunohistochemistry
MCHC	Mean corpuscular hemoglobin concentration
MRI	Magnetic resonance imaging
NHL	Non-Hodgkin Lymphoma
NK	Natural Killer Cell
PARR	PCR for antigen receptor rearrangements
CNSL	Central nervous system lymphoma
PCNSL	Primary central nervous system lymphoma
PCR	Polymerase chain reaction
T1-W	T1-weighted
T1w SE	T1-weighted spin echo
T1 GRE Turbo FLASH	T1-weighted, fat-suppressed, gradient-echo sequence
T2-W	T2-weighted
T2w FLAIR	T2-weighted fluid-attenuated inversion recovery
T2*-GRE	T2*-weighted gradient recalled echo
T2W TSE	T2-weighted turbo spin echo
TCR	T-cell receptor
TNF	Tumor necrosis factor
WHO	World Health Organization

1 Introduction and Problem Statement

Malignant lymphoma, originating from neoplastically transformed lymphocytes, represents a heterogeneous group of malignancies generally classified as Hodgkin lymphoma (HL) and non-Hodgkin lymphoma (NHL). These malignancies have the potential to infiltrate and accumulate in a wide range of tissues and organs throughout the body (1). Among them, central nervous system lymphoma (CNSL) is a rare subtype found in both veterinary and human medicine. CNSL is further classified into primary and secondary forms, based on its origin and disease progression (2).

The focus in the following case is on primary central nervous system lymphoma (PCNSL), which accounts for approximately for 1%–2% of NHL in humans (3) und 3% of all intracranial neoplasms in dogs (2). Although no definitive predisposition related to age, breed, or sex has been established for CNSL, a slightly higher prevalence has been reported in Labrador Retrievers and Rottweilers (4).

The clinical presentation of PCNSL is typically nonspecific, often encompassing a broad spectrum of neurological deficits such as cognitive decline, behavioral changes, gait abnormalities, or seizures (4). Consequently, a combination of diagnostic modalities including advanced imaging techniques, cerebrospinal fluid (CSF) analysis, blood work, and, in some cases, more invasive procedures such as tissue biopsies, is required to refine the differential diagnosis.

In veterinary medicine, however, there is a notable lack of standardized diagnostic protocols, not only für PCNSL, but for CNSL in general. The absence of standardized protocols limits the reliability of conclusions drawn about diagnosis, prognosis and treatment approaches (5).

This case report presents a diagnostically challenging case of PCNSL in a dog.

The aim of this study is to provide insights in opportunities and limitations of various diagnostic approaches, including clinical examination, magnetic resonance imaging, laboratory analyses, histopathology, and immunohistochemistry (IHC). Additionally, a brief overview of CNSL in different species is provided.

2 Literature review

2. 1 Tumors of the central nervous system

The classification of CNS tumors has traditionally been based on histological evaluation, supplemented by complementary techniques such as immunohistochemistry. Over the past decades, the classification system has undergone multiple revisions in response to scientific advancements and diagnostic possibilities. In an effort to provide a globally standardized framework, the World Health Organization (WHO) has published its fifth update on CNS tumor classification, incorporating the latest pathological insights. Importantly, as the WHO itself emphasizes, these classifications should be considered dynamic and continuously evolving, reflecting ongoing developments in research and diagnostics (1).

According to current knowledge, CNS tumors are now categorized based on a combination of defining molecular features, oncogenic pathways, histological and histogenetic characteristics, including the recognition of newly defined molecular subtypes. A current and detailed list of the classification of tumors of the CNS is presented in Table l, with hematolymphoid tumors discussed in more details below (6).

In veterinary neuro-oncology, the most common CNS tumors include meningiomas, astrocytomas, oligodendrogliomas, and choroid plexus tumors. Meningiomas are generally benign and exhibit a wide range of histological subtypes. Astrocytomas and glioblastomas represent a biologically diverse group of glial tumors, often characterized by infiltrative growth and histologic heterogeneity. Oligodendrogliomas, frequently observed in brachycephalic breeds, may appear as mixed tumors with astrocytic or ependymal differentiation. Choroid plexus tumors, including papillomas and carcinomas, are notable for their intraventricular localization and potential for CSF dissemination. Several rare and emerging entities, such as microgliomatosis, gliomatosis cerebri, polar spongioblastoma, and medulloepithelioma, contribute to the complexity of CNS tumor pathology in animals. Less common neoplasms include ependymomas, neuronal tumors, primitive neuroectodermal tumors, pineal region tumors, and lymphoid neoplasms such as PCNSL. These veterinary CNS tumors closely resemble their human counterparts in both histopathological features and biological behavior (7).

Table 1: Classification of brain and spinal cord tumors according to Louis et al. 2021 (Part I) (6).

Table 1 2021 WHO Classification of Tumors of the Central Nervous System. Provisional Entities are in Italics

World Health Organization Classification of Tumors of the Central Nervous System, fifth edition
Gliomas, glioneuronal tumors, and neuronal tumors
Adult-type diffuse gliomas
Astrocytoma, IDH-mutant
Oligodendroglioma, IDH-mutant, and 1p/19q-codeleted
Glioblastoma, IDH-wildtype
Pediatric-type diffuse low-grade gliomas
Diffuse astrocytoma, *MYB*- or *MYBL1*-altered
Angiocentric glioma
Polymorphous low-grade neuroepithelial tumor of the young
Diffuse low-grade glioma, MAPK pathway-altered
Pediatric-type diffuse high-grade gliomas
Diffuse midline glioma, H3 K27-altered
Diffuse hemispheric glioma, H3 G34-mutant
Diffuse pediatric-type high-grade glioma, H3-wildtype and IDH-wildtype
Infant-type hemispheric glioma
Circumscribed astrocytic gliomas
Pilocytic astrocytoma
High-grade astrocytoma with piloid features
Pleomorphic xanthoastrocytoma
Subependymal giant cell astrocytoma
Chordoid glioma
Astroblastoma, *MN1*-altered
Glioneuronal and neuronal tumors
Ganglioglioma
Desmoplastic infantile ganglioglioma / desmoplastic infantile astrocytoma
Dysembryoplastic neuroepithelial tumor
Diffuse glioneuronal tumor with oligodendroglioma-like features and nuclear clusters
Papillary glioneuronal tumor
Rosette-forming glioneuronal tumor
Myxoid glioneuronal tumor
Diffuse leptomeningeal glioneuronal tumor
Gangliocytoma
Multinodular and vacuolating neuronal tumor
Dysplastic cerebellar gangliocytoma (Lhermitte-Duclos disease)
Central neurocytoma
Extraventricular neurocytoma
Cerebellar liponeurocytoma
Ependymal tumors
Supratentorial ependymoma
Supratentorial ependymoma, *ZFTA* fusion-positive
Supratentorial ependymoma, *YAP1* fusion-positive
Posterior fossa ependymoma
Posterior fossa ependymoma, group PFA
Posterior fossa ependymoma, group PFB
Spinal ependymoma
Spinal ependymoma, *MYCN*-amplified
Myxopapillary ependymoma
Subependymoma

Table 1: Classification of brain and spinal cord tumors according to Louis et al. 2021 (Part II) (6).

Table 1 Continued

World Health Organization Classification of Tumors of the Central Nervous System, fifth edition
Choroid plexus tumors
Choroid plexus papilloma
Atypical choroid plexus papilloma
Choroid plexus carcinoma
Embryonal tumors
Medulloblastoma
Medulloblastomas, molecularly defined
Medulloblastoma, WNT-activated
Medulloblastoma, SHH-activated and *TP53*-wildtype
Medulloblastoma, SHH-activated and *TP53*-mutant
Medulloblastoma, non-WNT/non-SHH
Medulloblastomas, histologically defined
Other CNS embryonal tumors
Atypical teratoid/rhabdoid tumor
Cribriform neuroepithelial tumor
Embryonal tumor with multilayered rosettes
CNS neuroblastoma, *FOXR2*-activated
CNS tumor with *BCOR* internal tandem duplication
CNS embryonal tumor
Pineal tumors
Pineocytoma
Pineal parenchymal tumor of intermediate differentiation
Pineoblastoma
Papillary tumor of the pineal region
Desmoplastic myxoid tumor of the pineal region, *SMARCB1*-mutant
Cranial and paraspinal nerve tumors
Schwannoma
Neurofibroma
Perineurioma
Hybrid nerve sheath tumor
Malignant melanotic nerve sheath tumor
Malignant peripheral nerve sheath tumor
Paraganglioma
Meningiomas
Meningioma
Mesenchymal, non-meningothelial tumors
Soft tissue tumors
Fibroblastic and myofibroblastic tumors
Solitary fibrous tumor
Vascular tumors
Hemangiomas and vascular malformations
Hemangioblastoma
Skeletal muscle tumors
Rhabdomyosarcoma
Uncertain differentiation
Intracranial mesenchymal tumor, FET-CREB fusion-positive
CIC-rearranged sarcoma
Primary intracranial sarcoma, *DICER1*-mutant
Ewing sarcoma

Table. 1: Classification of brain and spinal cord tumors according to Louis et al. 2021 (Part III) (6).

Table 1 Continued

World Health Organization Classification of Tumors of the Central Nervous System, fifth edition
Chondro-osseous tumors
Chondrogenic tumors
Mesenchymal chondrosarcoma
Chondrosarcoma
Notochordal tumors
Chordoma (including poorly differentiated chordoma)
Melanocytic tumors
Diffuse meningeal melanocytic neoplasms
Meningeal melanocytosis and meningeal melanomatosis
Circumscribed meningeal melanocytic neoplasms
Meningeal melanocytoma and meningeal melanoma
Hematolymphoid tumors
Lymphomas
CNS lymphomas
Primary diffuse large B-cell lymphoma of the CNS
Immunodeficiency-associated CNS lymphoma
Lymphomatoid granulomatosis
Intravascular large B-cell lymphoma
Miscellaneous rare lymphomas in the CNS
MALT lymphoma of the dura
Other low-grade B-cell lymphomas of the CNS
Anaplastic large cell lymphoma (*ALK*+/*ALK*–)
T-cell and NK/T-cell lymphomas
Histiocytic tumors
Erdheim-Chester disease
Rosai-Dorfman disease
Juvenile xanthogranuloma
Langerhans cell histiocytosis
Histiocytic sarcoma
Germ cell tumors
Mature teratoma
Immature teratoma
Teratoma with somatic-type malignancy
Germinoma
Embryonal carcinoma
Yolk sac tumor
Choriocarcinoma
Mixed germ cell tumor
Tumors of the sellar region
Adamantinomatous craniopharyngioma
Papillary craniopharyngioma
Pituicytoma, granular cell tumor of the sellar region, and spindle cell oncocytoma
Pituitary adenoma/PitNET
Pituitary blastoma
Metastases to the CNS
Metastases to the brain and spinal cord parenchyma
Metastases to the meninges

Abbreviations: CNS, central nervous system; IDH, isocitrate dehydrogenase; NK, natural killer; PitNET, pituitary neuroendocrine tumor; SHH, sonic hedgehog.

2. 2 Hematopoietic CNS tumors

Hematopoietic malignancies comprise a group of proliferative disorders arising from lymphocytic, myeloid, or histiocytic cell origin. These neoplasms originate from pluripotent hematopoietic stem cells, which can differentiate into lymphoid and myeloid progenitor cells. These progenitors further develop into various mature blood cells lineages, such as erythrocytes, monocytes, granulocytes, megakaryocytes, and lymphocytes (8).

Hematopoietic tumors involving the CNS include lymphomas, neoplastic reticulosis, microgliomatosis, and histiocytic sarcoma. In veterinary medicine, these tumors are predominantly reported in dogs and cats, with occasional cases in ruminants (9). CNS lymphomas in animals most commonly occur as part of a multicentric systemic disease, rather than as isolated primary neoplasms (7).

Neoplastic reticulosis is a rare leukocytic malignancy, primarily reported in dogs and sporadically in cats, cattle, and horses. Clinically and histopathologically, it often resembles granulomatous meningoencephalitis (GME), showing a predominance of atypical histiocytic cell and high mitotic rates. Neoplastic reticulosis, however, is histologically characterized by large, angiocentric, histiocyte-like cells, moderate mitotic activity, and cellular atypia. Lesions are usually intraparenchymal, with a predilection for cerebral white matter. Immunohistochemically, these neoplastic cells are CD18-positive and negative for lymphocytic markers, indicating a non-lymphoid leukocytic origin (9).

Microgliomatosis in dogs is a rare, diffusely infiltrative CNS neoplasm, historically presumed to originate from microglial cells. Previously classified alongside neoplastic reticulosis due to its assumed mesenchymal origin, microgliomatosis is now distinguished by the absence of angiocentric growth. This disease occurs in mature and elderly dogs, presenting clinically with progressive cerebral dysfunction. Gross lesions are often subtle or absent, though diffuse white matter involvement may be noted. Histologically, microgliomatosis is characterized by widespread hypercellularity in the white matter of the cerebrum, brainstem, and cerebellum, with cells aligned along axonal pathways. These neoplastic cells are CD18-positive (9) and resemble microglia, displaying ovoid to rod-shaped basophilic nuclei with minimal cytoplasm (10). Subpial accumulations and perivascular sleeves may also be present, mimicking secondary structures seen in medulloblastoma (3).

Primary histiocytic sarcoma of the CNS has been reported in certain dog breeds, particularly the Bernese Mountain Dog and Golden Retriever. This neoplasm is marked by extensive infiltration and destruction of neural tissue by highly pleomorphic, often multinucleated large cells with abundant cytoplasm and frequent atypical mitotic appearance (3).

2. 2. 1 CNS lymphoma

2. 2. 1. 1 General considerations concerning lymphomas

Lymphomas are malignant neoplasms of the lymphoid system. While HL is characterized by the presence of Reed-Sternberg cells and occurs predominantly in humans, NHL represent a highly diverse group of malignancies that are of significant relevance in both human and veterinary medicine. NHL encompasses tumors derived from either immature or mature lymphoid cells of the B-cell, T-cell, or natural killer (NK)-cell lineages. B-cell and T/NK-cell lymphomas are clonal malignancies that arise at various stages of lymphocyte development. Although many of these tumors reflect identifiable stages of normal differentiation, not all neoplasms can be clearly aligned with a specific developmental phase. Due to overlapping immunophenotypic and functional characteristics, T-cell and NK-cell lymphomas are typically classified together. Furthermore, some lymphomas demonstrate lineage heterogeneity or rare lineage plasticity, complicating attempts to classify them based solely on their presumed normal counterpart (8).

Historically, NHL was referred to as lymphatic leukemia or lymphosarcoma, reflecting its systemic and proliferative nature. These tumors commonly originate in lymph nodes, the spleen, liver, and other lymphatic tissues, though extranodal manifestations are also frequently observed. In dogs, malignant lymphoma is a relatively common neoplasm and is anatomically classified into five main forms:

Multicentric lymphoma – involving multiple peripheral lymph nodes (most common)

Gastrointestinal lymphoma – affecting the stomach and/or intestines

Mediastinal lymphoma – primarily involving the thymus or mediastinal lymph nodes

Cutaneous lymphoma – affecting the skin (epitheliotropic or non-epitheliotropic)

Extranodal lymphoma – affecting organs such as the kidneys, eyes, or central nervous system (8).

Each form of lymphoma presents distinct clinical features and biological behavior, underscoring the importance of precise classification for effective therapeutic planning and accurate prognosis. In veterinary medicine, the classification of lymphoid neoplasms largely follows the framework proposed by the WHO (8), as adapted for animals in Jubb, Kennedy, and Palmer's Pathology of Domestic Animals, Sixth Edition (2015). This system advocates for a multifactorial diagnostic approach, incorporating morphological, immunophenotypic, molecular, and clinical criteria, in alignment with contemporary classification strategies used in human oncology (9).

2. 2. 2 CNS lymphomas in humans and different animal species

While lymphoma is a common form of cancer, PCNSL is rare, accounting for approximately 3 % (11) of all intracranial neoplasms and 4 % to 6 % of extranodal lymphomas in humans (12), cats (13) and dogs (11). The retrospective study by Fonti et al. (2023) revealed that intraparenchymal lymphomas were found in 27 % of dogs and 20,8 % of cats, often involving the forebrain with diffuse, non–mass-forming infiltration consistent with lymphomatosis cerebri. Intravascular lymphoma represented 45,4 % of canine CNS lymphomas was characterized by intraluminal proliferation of neoplastic cells, frequently causing thrombosis, necrosis, and hemorrhage. Extra-axial (meningeal) lymphomas were more common in cats (58,3 %) than dogs (9,1 %), with feline cases often presenting as primary B-cell tumors in the frontal leptomeninges. Leptomeningeal lymphomatosis was identified in both species, characterized by diffuse subarachnoid lymphocytic infiltration, sometimes extending into perivascular and subpial regions. Phenotypically, B-cell, T-cell, and non-B, non-T immunotypes were observed in both species. In dogs, B-cell lymphomas predominated among intraparenchymal cases, whereas feline lymphomas more often exhibited T-cell dominance (14).

A recent review found no specific age, breed, or sex predisposition in dogs for specific CNSL subtypes, although there was a slightly higher occurrence in Labrador Retrievers and Rottweilers (15). Canine CNSL is most likely comparable to the NHL in humans, and while it is well-documented in human medicine, there remains a significant lack of documentation and

research within the veterinary field. The etiology of canine lymphoma is unclear but likely involves a combination of genetic predisposition, environmental influences, and immunological dysregulation. For example, mutations in the tumor necrosis factor (TNF) receptor-associated factor 3 gene have been identified in nearly 44 % of a specific subtype of diffuse large B-cell lymphoma (DLBCL), resulting in dysregulation of the transcription factor NF-kB in neoplastic cells. Potential exogenous carcinogens include exposure to magnetic fields, lawn-care chemicals, and living near industrial waste-incineration or radioactive sites. Chronic inflammation, immunosuppression, and autoimmune diseases have also been implicated as endogenous risk factors (8).

Clinical manifestations of CNSL vary significantly with lesion location and extent but most commonly includes seizures and behavioral changes (11), gait abnormalities (16), and various other neurological deficits (17). Central diabetes insipidus has also been reported in association with the disease (18).

2. 2. 3 Diagnostic pathways for CNS lymphomas

Given the heterogeneity of clinical presentation and the continued absence of standardized diagnostic guidelines, the diagnosis of CNSL in dogs requires a multi-step approach that combines several diagnostic tools and techniques. Each step should be guided by the patient's clinical signs and the resulting presumptive diagnosis. This begins with a thorough patient history, followed by a comprehensive physical and neurological examination. The neurological examination aims to localize the lesions to one of four major brain regions: forebrain, midbrain, pons/medulla, or cerebellum. Accurate localization at this level is usually sufficient to refine differential diagnoses and plan further testing. Clinicians must decide whether the presentation suggests focal, diffuse, or multifocal disease. Focal lesions - often indicated by lateralizing signs such as circling or focal seizures - commonly suggest neoplasia, vascular events, or localized infections. In contrast, diffuse lesions typically point to metabolic, toxic, or degenerative conditions. However, focal lesions can mimic diffuse disease through secondary effects such as edema or hydrocephalus. Multifocal disease should be considered when all clinical signs cannot be explained by a single lesion, (19).

With a particular focus on CNS, the most common utilized imaging modalities are computed tomography (CT) and magnetic resonance imaging (MRI), with the latter generally preferred

in both canine and feline patients. Although meningiomas (11) and histiocytic sarcomas (20) may exhibit characteristic changes on MRI, these findings, including those seen in CNSL, are not specific. Nevertheless, CT and MRI provide critical diagnostic information when correlated with clinical signs (8).

CNSL lesions characteristically appear isointense to hypointense on T1-weighted (T1-W) images and hyperintense on T2-weighted (T2-W) images (21, 22). These lesions often demonstrate moderate to strong contrast enhancement, which is usually homogeneous but can vary depending on the lesion's characteristics. These abnormalities can appear well- or ill-defined, singular or multifocal, and may involve both intra-axial and extra-axial locations. Additionally, CNSL is frequently associated with perilesional edema and mass effect, both of which contribute to the observed clinical presentation (23).

Routine laboratory tests are essential, non-invasive diagnostic tools that assist in identifying infections, metabolic disturbances, or toxin exposure, but may also reveal a broad spectrum of non-specific changes (16). A complete blood count (CBC) may indicate infectious or inflammatory processes and can provide insight into other underlying conditions. A serum biochemistry profile and urinalysis are critical for detecting energy imbalances, electrolyte abnormalities, or the accumulation endogenous toxins. Liver function assessment, particularly bile acids testing or an ammonia tolerance test, is particularly important in animals presenting with seizures or clinical signs of diffuse forebrain involvement. Because neurologic signs can also result from endocrine disorders such as hypothyroidism, hyperadrenocorticism, or insulin-secreting tumors, a thorough endocrine evaluation should be performed when supported by clinical findings (19).

CSF analysis provides valuable insight into the cellular and biochemical environment of the central nervous system. The detection of a high number of neoplastic lymphoid cells in the CSF, combined with an elevated protein concentration is considered diagnostic for CNSL (17).

However, two important challenges must be considered. First, reference values for CSF parameters can vary between laboratories and across different literature sources, potentially complicating interpretation. Second, CSF collection is an invasive procedure that carries risks such as brain herniation in patients with increased intracranial pressure. Additionally, CSF may

be unsuccessful due to significant blood contamination or a “dry tap”, where no fluid is retrieved (19).

CSF can also be examined using polymerase chain reaction (PCR), a highly sensitive technique that rapidly and efficiently replicates nucleic acids. PCR is invaluable for the direct detection of CNS pathogens, such as bacteria, viruses, and fungi (24). In addition to identifying infectious agents, PCR clonality testing, specifically PCR for antigen receptor rearrangement (PARR), helps to distinguish reactive, polyclonal lymphocytic infiltrates from neoplastic mono- or oligoclonal proliferations. PARR can be applied to both B- and T-cell lymphocyte populations (25), differentiating benign lymphoid proliferations from malignant lymphoma (10). It assesses the genetic diversity within a lymphocyte population by examining the rearrangement of B-cell (IgH) or T-cell (TCR) receptor genes (10).

More precise insight is offered by pathological examinations, including histopathology and immunophenotyping. Histology involves the microscopic evaluation of tissue samples and offers direct evidence of lymphoma by revealing malignant lymphocytic infiltration. This method is essential for distinguishing CNS lymphoma from other primary CNS neoplasms, as clinical and imaging findings may overlap. Furthermore, histopathology enables the accurate classification of lymphoma into specific subtypes. Building on this, IHC serves as an indispensable adjunct to histology. IHC is an antibody-based method to detect lineage-specific proteins, providing immunophenotypic information. This not only complements histopathologic findings but also has significant implications for treatment decisions and prognosis (5).

2. 2. 4 Treatment and prognosis of CNS lymphomas

In human medicine, established protocols and clinical experience guide therapeutic decisions. This involves various chemo-immunotherapy combinations and autologous stem cell transplantation, which makes the disease potentially curable (26). By contrast, managing canine CNS lymphoma, particularly PCNSL, remains challenging due to significant diagnostic and therapeutic limitations, compounded by owner compliance. Historically, a definite diagnosis in dogs has been achieved mainly postmortem, due to non-specific clinical signs and

inconclusive imaging findings. These diagnostic hurdles directly affect treatment options and limit the ability to determine a reliable prognosis (27).

A recent case report describing two dogs with CNS lymphoma applied therapeutic approaches analogous to those used in human medicine; however, the authors emphasized the need for further optimization, particularly in establishing an effective (chemo-)therapy protocol for B-cell lymphomas (28). Beyond these two isolated cases, the veterinary literature consists mainly of retrospective studies (11) and literature reviews, which provide only limited prognostic insight (27).

3 Material and Methods

3. 1 Case Description

A 9-year-old neutered male mixed-breed dog, weighing 20 kg, was presented to the Emergency Unit of the University of Veterinary Medicine, Vienna with a two-week history of progressively worsening ataxia, behavioral changes, and swallowing difficulties.

During the initial clinical examination, all vital parameters were within normal limits. Visual inspection, however, revealed a swaying gait with noticeable crossing of the forelimbs. The initial neurological assessment identified proprioceptive and spinal-reflex abnormalities. Specifically, hopping and placing reactions of the left forelimb were mildly delayed, while both the patellar reflex and the cranial tibial muscle reflex were exaggerated in both hind limbs. In contrast, the extensor carpi radialis reflex of the left forelimb was mildly diminished. Anisocoria was observed, more pronounced in the right eye, accompanied by a delayed and incomplete pupillary light reflex.

During the examination, the dog's gait became increasingly unsteady until it collapsed onto its left side. At this point, a rapid nystagmus, alternating between horizontal and rotary phases, was observed and lasted approximately 20 seconds. A second, similar episode occurred roughly 30 minutes later, during which the nystagmus initially presented as horizontal before becoming rotary. This episode, like the first, lasted less than 30 seconds.

During the neurological examination the following morning, a significant clinical deterioration was evident. The patient presented in a markedly reduced general condition, with minimal response to manipulation or external stimuli, and diminished pain perception. Although the dog could still be assisted into a standing position, walking and standing independently were no longer possible. Consequently, proprioception could only be partially assessed, revealing a generalized moderate reduction in overreaching responses.

Assessment of spinal reflexes showed a mildly reduced patellar reflex bilaterally and a moderately increased cranial tibial muscle reflex. Pupillary reflexes were incomplete bilaterally. Additional cranial nerve deficits included moderate bilateral ventral strabismus, vertical nystagmus, and a more pronounced left-sided facial nerve paralysis (facial paresis). The Glasgow Coma Scale yielded a total score of 14.

The patient's condition remained largely unchanged and poor throughout the following day. General responsiveness remained reduced, though the patient reacted to active verbal engagement. Walking and standing without additional assistance were still not possible. Food and water intake required supervision and assistance, and the patient's appetite progressively declined. On lung auscultation, diminished vesicular breath sounds were noted on the right side. Given the pre-existing swallowing difficulties, these findings raised suspicion of an early-stage aspiration pneumonia.

With a presumptive diagnosis of an intracranial process, the patient was transferred to the intensive care unit (ICU) for stabilization, close monitoring, and to proceed with diagnostic imaging, including CSF analysis.

Stabilization therapy consisted of intravenous fluid administration (3 mL/kg/h, i.v. Sterofundin®, Braun, AT), gastroprotection and intracranial pressure management with esomeprazole (1 mg/kg i.v. BID Esomeprazol® STADA, STADA Arneimittel GmbH, AT), antiemetic treatment with maropitant (1mg/kg i.v. SID Prevomax®, Dechra, NL), and analgesia with metamizole (20mg/kg i.v. TID, Novasul®, VetViva Richter, AT). Midazolam (0.2 mg/kg i.v., Midazolam Actavis, Actavis Deutschland GmbH & Co. KG) was administered as needed for anticonvulsant therapy.

The monitoring protocol included continuous seizure surveillance and regular assessments of vital parameters at 4-hour intervals, hourly respiratory rate monitoring, electrocardiogram (ECG) monitoring, non-invasive blood pressure measurements, continuous oxygen saturation monitoring, and venous blood gas analyses at regular intervals throughout the entire hospital stay.

Within one hour of medication administration, a decline in general condition was noted, accompanied by a mild increase in body temperature from 38.6 °C to 39.1 °C). In response, the intravenous fluid therapy was adjusted, switching from a balanced isotonic crystalloid solution (3 mL/kg/h, i.v. Sterofundin®, Braun, AT) to an alternative isotonic solution (ELO-MEL®, Fresenius Kabi Austria GmbH, AT). The internal body temperature remained elevated at 39.1 °C despite administration of metamizole.

3. 2 Diagnostic procedures

For MRI and CSF collection, the dog was placed under general anesthesia. The anesthesia protocol was butorphanol (0.2 mg/kg i.v., Butormidor®, VetViva Richter GmbH, AT) was used for premedication, propofol (1-4 mg/kg i.v., Propofol "Fresenius", Fresenius Kabi Austria GmbH, AT) for induction, and sevoflurane (2.0-3.5% end-tidal sevoflurane) for maintenance. As infusion therapy a balanced isotonic crystalloid solution (i.v., Sterofundin®, Braun, AT) was administered at a flow rate of 10 mL/kg/h. Anesthesia lasted 110 minutes. A tachycardia (heart rate > 200 bpm) developed as a complication and was treated with dexmedetomidine hydrochloride (0.25 µg/kg i.v., Sedadex®, Dechra, NL). The mean heart rate ranged between 80 and 100 bpm, mean non-invasive blood pressure remained 70-90 mmHg. Pulse oximetry indicated oxygen saturation values of 95-100 %, while capnography showed mean $ETCO_2$ levels of 40-50 mmHg, and a mean respiratory rate of 10-20 breaths/min. The mean core body temperature remained between 38-39 °C throughout anesthesia. The patient was mechanically ventilated using "The Leon" anesthesia workstation (Löwenstein Medical Austria GmbH, AT). At the end of the procedure, atipamezole hydrochloride (0.1 mg/kg i.m. Antisedan®, Orion Corporation, FI) was administered for reversal. The recovery phase went uneventful.

3. 2. 1 MRI

MRI scans of the head were performed using a 1.5 T device (Siemens Magnetom Espree, Siemens Healthcare, Erlangen, Germany) under general anesthesia. T2-weighted turbo spin echo (T2w TSE) images were acquired in three planes to assess general brain anatomy and pathology. Transverse T2-weighted fluid-attenuated inversion recovery (T2w FLAIR) sequences were used to identify lesions with high water content while suppressing CSF signals. T2*-weighted gradient recalled echo (T2*-GRE) was included to detect hemorrhage or mineralization. T1-weighted spin echo (T1w SE) images were obtained prior to contrast administration, followed by three-plane post-contrast T1w SE sequences to access lesion enhancement. Additionally, a 3D T1-weighted, fat-suppressed, gradient-echo sequence (T1 GRE TurboFLASH) was performed to provide high-resolution anatomical detail. Diffusion-weighted imaging (DWI) was conducted in both transverse and dorsal planes with fat saturation, and corresponding apparent diffusion coefficient (ADC) maps were generated to evaluate tissue diffusivity and identify areas of restricted diffusion.

3. 2. 2 Laboratory diagnostics

3. 2. 2. 1 Blood analysis

Blood examination during hospitalization included hematology and differential blood count using the Advia 2120i (Siemens Healthineers, DE), and blood chemistry performed using the Cobas c501 (Roche Diagnostics, CH).

3. 2. 2. 2 CSF analysis

The evaluation of CSF included assessment of its color, total cell count, and possible blood contamination, as well as t the Pandy test. Additionally, measurements of pH, osmolality, and cytological composition were conducted.

CSF processing and evaluation followed these guidelines:

- Physiologically, CSF is colorless. When a reddish discoloration is observed, the sample should be centrifuged at low speed (1000–1500 rpm) for five minutes. The supernatant is then re-evaluated. A clear supernatant suggests blood contamination due to a traumatic puncture. Conversely, persistent reddish to yellowish discoloration of the supernatant is indicative of a prior (non-iatrogenic) hemorrhage.

- The clarity of the CSF is normally assessed as clear. Deviations from this are graded semi-quantitatively: slight opalescence is noted as '+', moderate turbidity as '++', marked turbidity with a milky appearance as '+++', and the presence of visible precipitate as '++++'.

- For cell count analysis, 10 µL of Samson's solution (Morphisto GmbH, DE) and 100 µL of CSF are mixed into a 1.5 mL reaction vessel. The mixture is gently mixed and incubated on a roller mixer at room temperature for 10 minutes. Subsequently, the sample is transferred to a Fuchs-Rosenthal counting chamber and evaluated after 3 minutes under 400× magnification with the condenser aperture closed. All nucleated cells are counted, and the final result is expressed as one-third of the total count. Special

attention is given to the presence and morphology of mononuclear, polymorphonuclear, and atypically altered cells or nuclei.

- Osmolality is measured using an osmometer, while pH is determined with an indicator strip (urine test strip).

- The Pandy reaction (or Pandy test) is a semi-quantitative method to determine protein content in CSF. For this purpose, 200 µL of Pandy reagent is mixed with up to 100 µL of the CSF sample in a watch glass. Proteins, particularly globulins, react with the saturated carbolic acid solution - usually a saturated phenol - resulting in a turbidity that correlates with the protein concentration. The turbidity is assessed against a dark background and graded semi-quantitatively as previously described. The presence of turbidity indicates a positive test result.

- The Nonne-Appelt test, which is performed only if the Pandy test yields a positive result, is used to differentiate between albumin and globulin in CSF. The test primarily detects the presence of globulins, which precipitate when a saturated ammonium sulfate solution is added. This protein precipitation results in visible turbidity, the extent of which correlates with an elevated globulin concentration in the CSF. Albumin, by contrast, remains largely in solution and is not reliably detected by this method.

- Microscopic evaluation includes the determination of cell count and cell types, estimation of the relative proportions of different cell populations, and detecting microorganisms, contaminants, or crystals.

- For CSF chemistry analysis, including t total protein and glucose concentrations, the sample is centrifuged at 10,000 rpm for 3 minutes. Subsequently, relevant parameters are measured using the Cobas c501 analyzer (Roche Diagnostics, CH).

3. 2. 3 Pathology

3. 2. 3. 1 Histopathology

For histopathology, representative samples of numerous tissues including brain were fixed in 10% neutral-buffered formalin and embedded in paraffin-wax for histopathological examination. The tissue blocks were cut into 2 µm sections and were routinely stained with hematoxylin and eosin (HE). To further characterize the nature of the infiltrating cells, toluidine blue staining was also performed.

3. 2. 3. 2 IHC

Immunohistochemical analysis was performed to further classify the lymphoma identified on histopathology. The following primary antibodies were used: CD3 as a T cell marker, CD79a for B cell/plasmacytoid lesions, Iba-1 and Pax-5 to confirm or rule out histiocytes, as well as Granzyme B and CD56 for further subtypes, i.e. NK-cells and large granular lymphocytes, respectively.

Avidin-biotin complex technique was performed manually (CD 56, Granzyme-B) or automatically (CD3, CD79a, Iba-1, Pax-5) on an Autostainer (EprediaLab Vision Autostainer 360, Runcorn, UK) respectively. Formalin-fixed, paraffin-embedded brain sections (2 µm) of allocortex/olfactory bulb, cerebellum/pons, and hippocampus were placed on coated slides. Antigen retrieval was performed on deparaffinized and rehydrated sections without pretreatment (Iba-1) or by heat-pretreatment (see Table 2). For the automatically performed antibodies, endogenous peroxidase activity was blocked by incubation in 3 % H_2O_2 solution, interfering background staining was reduced by using 1.5 % normal goat serum (Invitrogen/Thermo Scientific, USA) as a protein blocker. Manually, endogenous peroxidase activity was blocked by 0.6 % methanol/H_2O_2. Subsequently, the primary antibodies (see Table 2) were applied and incubated with the BrightVision detection system (BrightVision poly-HRP-anti-mouse IgG or BrightVision poly-HRP-anti-rabbit IgG; ImmunoLogic, NL); the resulting complex was visualized by adding BrightDAB (ImmunoLogic, NL) as chromogen or DAB Quanto (Thermo Scientific, US) for the manually performed antibodies CD56 and Granzyme B, respectively. Contrast counterstaining with hematoxylin was performed. Finally, the sections were dehydrated and mounted. A canine lymph node served as positive control for CD3, CD79a

and Pax-5, while brain tissue from a pig served as positive control for Iba-1, and a feline spleen for CD56 and Granzyme B.

Table 2: Antibodies used for immunohistochemical investigations.

Primary Antibody	Source	Dilution	Antigen retrieval
Rabbit polyclonal CD3	Dako, DK (A0452)	1:1000	Heating in citrate buffer pH 6
Mouse monoclonal CD79a [HM47/A9]	Abcam, UK (ab3121)	1:1500	Heating in EDTA buffer pH8
Mouse monoclonal B-cell-specific activator protein (Pax-5)	Dako, DK (M7307)	1:100	Heating in citrate buffer pH 6
Rabbit polyclonal Iba-1	Wako, Japan (019-19741)	1:1000	No pretreatment
*Mouse monoclonal CD56 (Clone 1G4]	LSBio, US (LS-B12970-50)	1:150	Heating in citrate buffer pH6
*Rabbit polyclonal Granzyme B	Abcam, UK (ab4059)	1: 400	Heating in citrate buffer pH6

* manually performed

4 Results

4. 1 MRI

The imaging protocol was tailored to optimize visualization of intracranial structures and assess for potential pathological changes. The neurocranial structures appeared normal. The midline was preserved, and the ventricular system, gyri, and sulci were of normal width and symmetrical in both hemispheres. The craniocervical junction was also unremarkable. No abnormal signal intensities or contrast enhancement were detected within the brain parenchyma or surrounding meningeal spaces across all sequences and planes.

The splanchnocranium also demonstrated largely unremarkable findings. A mild fluid accumulation was observed in the right tympanic bulla, with no associated signal changes or evidence of mucosal thickening or contrast enhancement suggestive of bulla lining inflammation. The left tympanic bulla, external and internal ears, and salivary glands appeared normal. The temporomandibular joints were congruent and exhibited no changes. Similarly, no pathological signal intensities or contrast enhancement were detected in the nasal cavity and paranasal sinuses.

In conclusion, MRI revealed no intracranial abnormalities or pathological changes. The mild right-sided middle ear effusion was considered incidental (Fig. 1, 2).

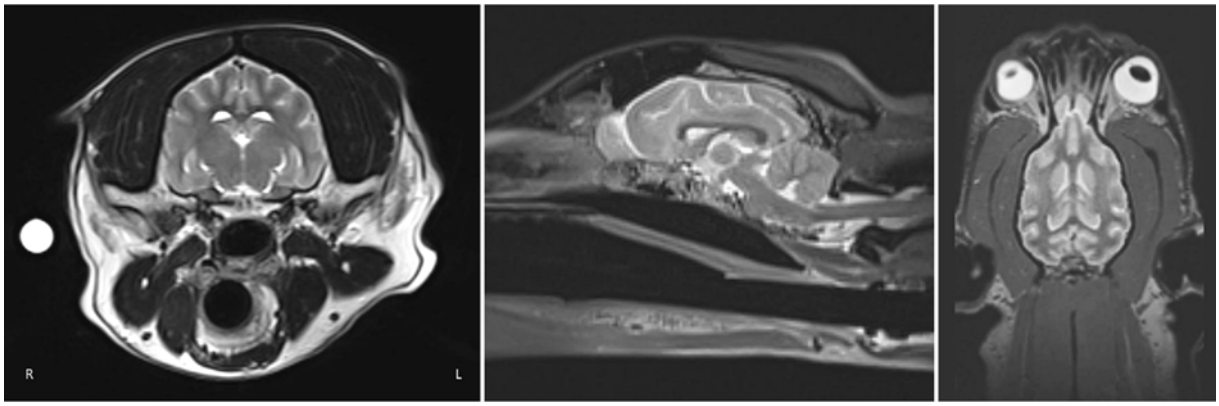

Fig. 1: T2-weighted turbo spin echo (T2w TSE), 3D sequences. Representative slices of the patient's brain in axial (left), sagittal (center), and dorsal (right) planes. All images show normal intracranial anatomy without evidence of abnormal signal intensities, mass lesions, or structural deviations.

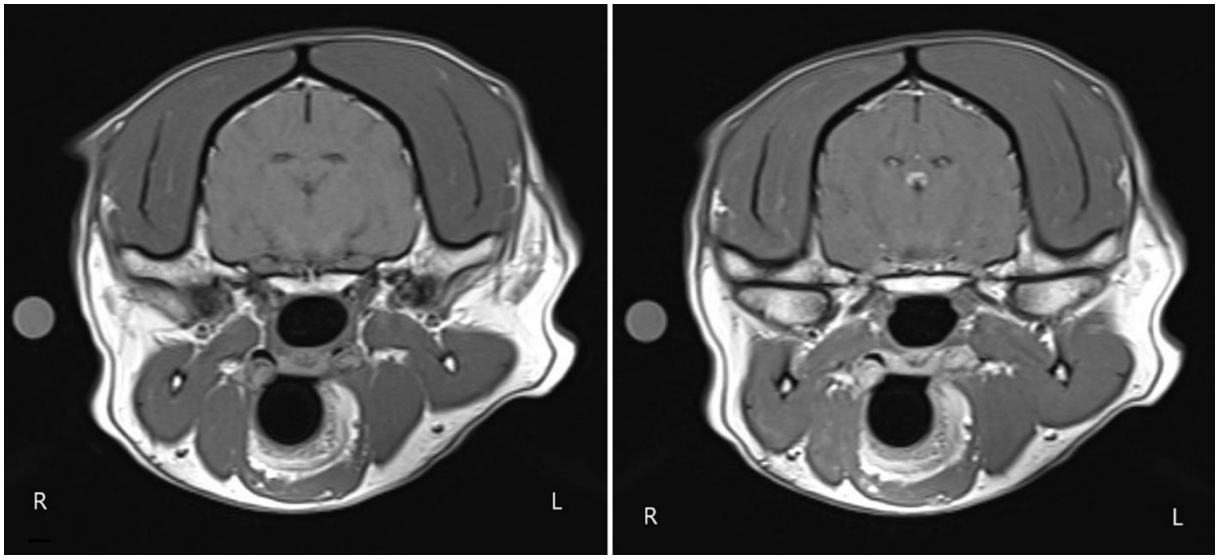

Fig. 2: T1-weighted spin-echo (T1w SE) axial images of the brain before (left) and after (right) intravenous gadolinium-based contrast administration.

Both pre- and post-contrast images show no abnormal parenchymal or meningeal enhancement. The ventricular system and midline structures are preserved, with no evidence of mass effect or intracranial pathology.

4. 2 Laboratory findings

4. 2. 1 Blood analysis

The hematological examination revealed erythropenia (5.09 × 10^6/µL; reference range: 5.50-8.00), hypochromasia with a hemoglobin level of 11.4 g/dL (reference range: 12.0-18.0), and hypohematocritemia (hematocrit: 33.1 %; reference range: 37.0-55.0 %). Additionally, an increased mean corpuscular hemoglobin concentration (MCHC) of 34.4 g/dL (reference range: 31.0-34.0) was noted. Further findings included neutrophilia (78 %; reference range: 55.0-75.0) and monocytosis (8.3 %; reference range: <5.0).

Biochemical analysis showed hypouricemia (19.6 mg/dL; reference range: 20.0-40.0) and hypoproteinemia (4.65 g/dL; reference range: 6.00-7.50).

Venous blood gas values are summarized in Table 3.

blood gas values	result 1	result 2	result 3	unit	reference range
pH	7.42	7.38	7.39		7.351-7.463
pCO2	27.20*	36.00	37.20	mmHg	32.0-49.0
pO2	62.60	64.80	50.70	mmHG	24.0-48.0
cHCO3	16.90	20.50	21.40	mmol / L	18.0-24.0
BEecf	- 7.14	- 4.20	- 3.06	mmol / L	-2.5 - +2.5
BE	- 4.87	- 3.46	- 2.52	mmol / L	-2.5 - +2.5
Na+	145.40	145.30	141.30	mmol / L	140.0-152.0
K+	4.44	4.08	3.86	mmol / L	3.6-5.6
Ca2+	1.20	1.24	1.28	mmol / L	1.120-1.420
Cl-	117.60	117.70	113.20	mmol / L	95.0-113.0
AnGap	15.00	11.00	10.00	mmol / L	12-24
Glu	72.00	85.00	74.00	mg / dL	55-90
Lac	2.30	0.90	0.90	mmol / L	< 1.0
tHb	17.30	11.70	10.20	%	
SO2	96.50	95.80	84.40	%	
O2Hb	86.80	86.20	76.20	%	
COHb	8.50	8.50	8.30	%	
MetHb	1.50	1.50	1.40	%	
HHb	3.20	3.80	14.10	%	

Table 3: Blood gas values. Result 1: measured right after admission; result 2 six hours after result 1; result 3: 24h after result 1; *numbers in red indicate abnormal values.

4. 2. 2 CSF analysis

The CSF was colorless and clear in appearance. A markedly elevated cell count of 1489/3 µL (reference: < 15) was observed, accompanied by significant blood contamination.

Cytological examination revealed approximately 99 % pleomorphic mononuclear cells with variable amounts of cytoplasm, round to pleomorphic nuclei, prominent nucleoli and cytoplasmic blebs, occasionally appearing rounded. Rare small lymphocytes and occasional eosinophils were also present. Although the cytological appearance was not entirely conclusive, the cellular morphology was considered highly suspicious for lymphoma.

The CSF total protein concentration was 45.4 mg/dL (reference: < 48.0 mg/dL) and glucose concentration was within normal limits at 52.0 mg/dL (reference: 40.0-70.0 mg/dL); Pandy's reaction was negative, pH was elevated at 9.00, and osmolality measured 303 mOsm/kg. These findings, particularly the marked pleocytosis with monomorphic cell population and

morphologic features suggestive of neoplasia, support a differential diagnosis of central nervous system lymphoma.
According to those CSF findings, which implicated a poor prognosis, the owners decided against further treatment and chose euthanasia.

4. 3 Pathological findings

4. 3. 1 Necropsy

Postmortem examination revealed no major external abnormalities, aside from a few small, subcutaneous lipomas. In the thoracic cavity, there was a mild serous effusion, along with moderate eccentric left ventricular hypertrophy with small lymphocytic and fibrotic foci, discrete fibrosis of the mitral valves, and moderate congestive hyperemia. Additionally, small submucosal hemorrhages were noted in the larynx and the upper sections of the trachea.
In the abdominal cavity, the liver displayed signs of subacute congestion, and the left kidney showed evidence of mild chronic interstitial nephritis with focal infarct scars. The spleen was moderately hyperemic, and the gastrointestinal tract was unremarkable apart from small submucosal hemorrhages in the jejunum. The prostate was notably small, comparable in size to a cherry.

4. 3. 2 Histopathology

Although the brain appeared macroscopically unremarkable during necropsy, histological examination revealed diffuse perivascular lymphoid cell infiltration throughout the neuroparenchyma, as well as within the meninges, choroid plexus, and selected cranial nerve segments (Fig. 3, 4).
The infiltrating lymphoid cells were characterized by large, occasionally polygonal morphology, with abundant cytoplasm and predominantly round to occasionally bean-shaped nuclei. The nuclei showed variable chromatin patterns with exhibited prominent nucleoli. Overall, there was marked anisocytosis and anisokaryosis (Fig. 5).
Some cells appeared to contain granules within their cytoplasm, in which case mast cell involvement should be considered. However, toluidine blue staining, a standard method for mast cell identification, was negative.

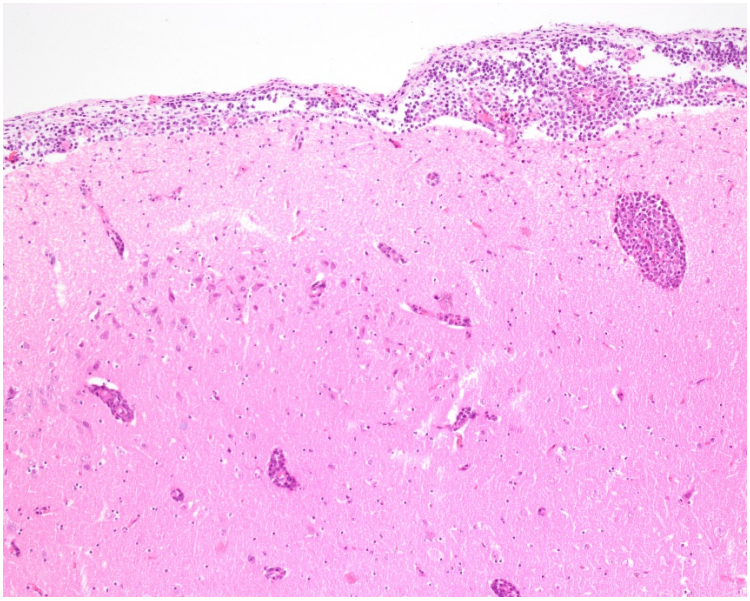

Fig. 3: Thickening of leptomeninges due to massive infiltration of lymphoid cells; furthermore, perivascular lymphoid cuffing in adjacent brain tissue. Olfactory bulb, HE, 10x.

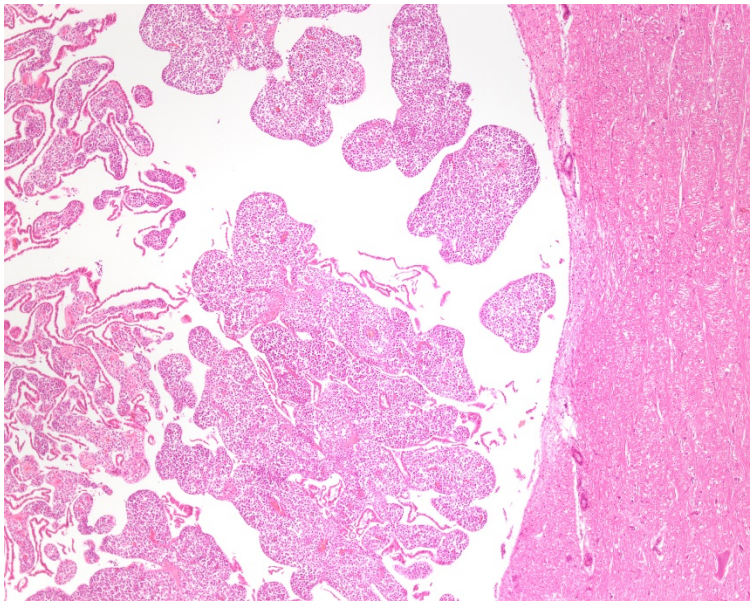

Fig. 4: Highly thickened choroid plexus due to lymphoid infiltration. Fourth Ventricle, HE, 4x.

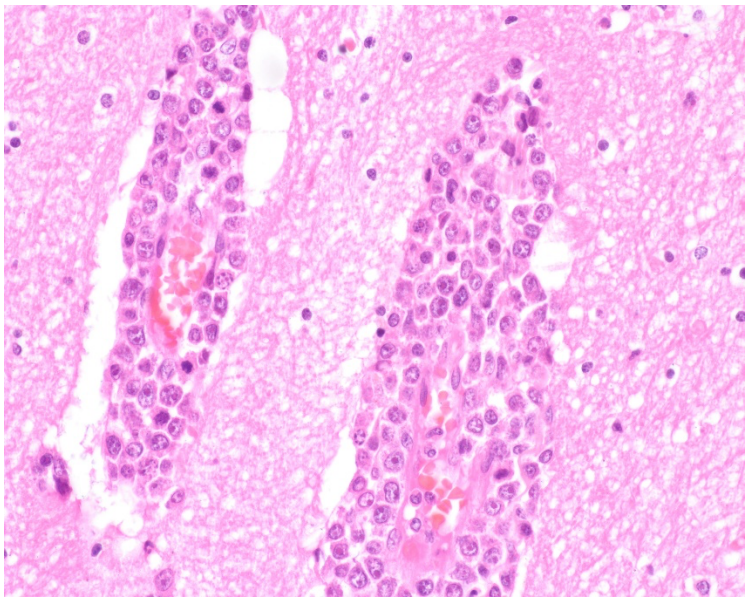

Fig. 5: Lymphoid cells form broad perivascular cuffs. Note massive anisokaryosis and anisocytosis. Olfactory bulb, HE, 40x.

4. 3. 3 IHC

IHC revealed scattered single cells positive for CD3, CD79a, Pax-5 and Iba-1. However, the vast majority of infiltrating tumor cells remained negative for all these markers (Fig. 6), in strong contrast to the respective positive control tissues (Fig. 7). Additionally, immunostaining for CD56 and Granzyme B yielded negative results across the entire lymphoid population in the brain.

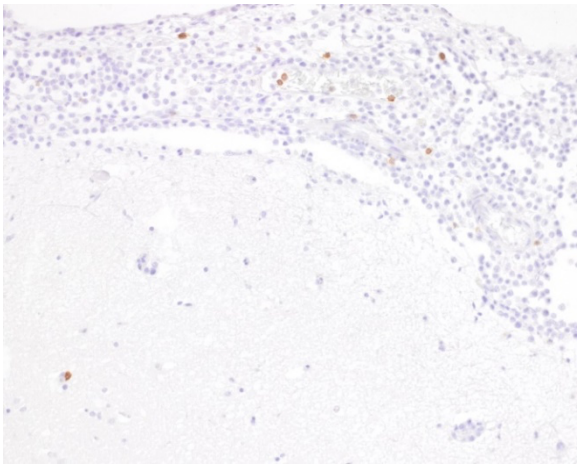

Fig. 6: Single CD-3 immunopositive cells interspersed within the dense meningeal neoplastic infiltrates. Olfactory bulb, IHC, 20x.

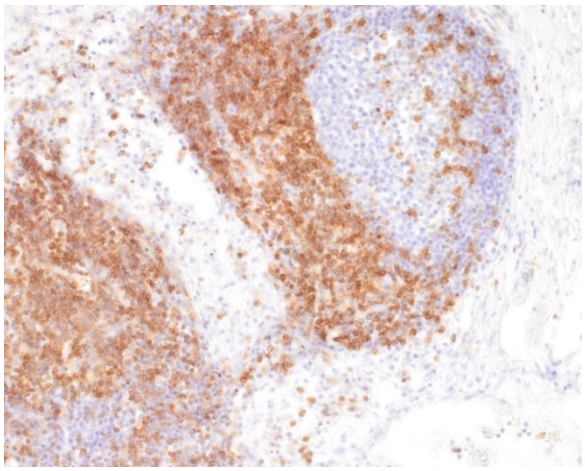

Fig. 7: Positive control for CD3. Note deeply brownish immunostaining at the follicle periphery, characteristic for T cells. Lymph node, IHC, 20x.

5 Discussion

The present case report describes an unusual presentation in a nine-year-old, male-neutered mixed-breed dog with progressive neurological symptoms, including altered gait, mentation changes, and dysphagia. A thorough clinical and neurological examination, complements by routine blood work, raised suspicion of an intracranial process. Consequently, advanced diagnostic imaging, including MRI and CSF analysis, was conducted to further investigate potential intracranial lesions.

CSF analysis remains a key component in the diagnostic workup of CNS disease, particularly in cases where underlying lymphoproliferative or inflammatory processes are presumed (29). Findings such as pleocytosis, elevated protein concentration, and the presence of atypical lymphoid cells supported the suspicion of PCNSL in the presented dog. PCNSL is a rare form of malignant lymphoproliferative disease restricted to the CNS in dogs (11). Due to its intracranial location and frequently nonspecific clinical signs, including seizures, ataxia, altered mentation, or behavioral changes (17), diagnosis is often challenging, as it was in the current case.

Though there was an elevated cell count providing crucial evidence for an underlying malignant process, a definitive diagnosis would have typically required additional diagnostic laboratory modalities, such as PARR. PARR is valuable in distinguishing between reactive (polyclonal) and neoplastic (monoclonal) lymphoid populations, and is especially useful in cases with inconclusive cytology or limited cellularity (20, 21).

A potential limitation in CSF-based diagnostics lies in the sample volume. Unlike venipuncture, re-sampling of CSF is often not feasible due to the relatively invasive and technically demanding nature of the procedure. In the present case, there was insufficient residual material available following cytological and biochemical analysis to perform PARR. Furthermore, hematological evaluation and biochemical analysis revealed moderate but nonspecific changes, possibly indicating a chronic inflammation or paraneoplastic process. However, these findings provided no conclusive evidence of major organ disfunction or lymphoproliferative disease.

One unusual aspect of this case was the complete absence of MRI abnormalities. In most reported PCNSL cases, lesions appear isointense to hypointense on T1-W images and hyperintense on T2-weighted T2-W images and frequently exhibit restricted diffusion on DWI because of their high cellularity (21, 22, 30). In this case, however, all standard sequences, including T1-W, T2-W, and post contrast imaging, were completely unremarkable. This finding highlights a significant diagnostic limitation of MRI in certain PCNSL, although MRI is considered the gold standard for brain imaging (23). Consequently, the case underscores the importance of integrating additional diagnostic methods, such as CSF analysis.

The postmortem examination revealed only mild systemic alterations, including moderate cardiac changes and submucosal hemorrhages in the larynx and jejunum. Notably, there was no enlargement of spleen, liver or lymph nodes, and no gross evidence of disseminated lymphoproliferative disease.

Although the brain appeared macroscopically unremarkable, histopathology confirmed the CSF-based suspicion of PCNSL. Diffuse infiltration by large, atypical lymphoid cells with abundant cytoplasm and prominent nucleoli was observed primarily in the leptomeninges, including the cranial nerves and choroid plexus, while lymphoid infiltration of neuroparenchyma was limited to perivascular spaces adjacent to the meninges, and restricted to the superficial cortical layers. This kind of infiltration may explain the lack of detectable MRI abnormalities, as no solid tumor masses, obvious lymphoid cell aggregates or significant perilesional edema were present, features that typically contribute to visibility on standard MRI sequences (23). Meningitis and encephalitis, however, are generally detectable on MRI and are characterized by diffuse cellular infiltration (31). The failure to visualize these extensive lymphoid infiltrates on imaging remains an unresolved diagnostic challenge and highlights the limitations of MRI in certain forms of meningeal involvement.

IHC plays an important role in tumor characterization. The use of specific tumor markers, such as CD3 for T cells and CD79a for B cells, enables accurate immunophenotyping of neoplastic cells, and aids in establishing cellular origin of lymphoproliferative disease. In the present case, however, IHC yielded only sparse positivity for CD3 and CD79a, limited to single cells, while

the majority of infiltrating lymphoid cells remained immunonegative. Immunostaining with CD56 and Granzyme B markers for NK cells and T-cell subsets, also returned negative results.

Notably, PCNSL in dogs has been reported to frequently lack expression of standard IHC markers such as CD3 and CD79a (32), a phenomenon not fully reflected in the current literature (9, 21). This discrepancy may be attributed to a broad biological variability among canine lymphomas. To address this, comprehensive immunohistochemical studies are needed to investigate marker expression profiles and to diagnostic accuracy in these cases.

Despite a clear immunophenotypic profile in this case, tumor cell morphology strongly supports the diagnosis of lymphoma, most probably B-cell lymphoma, which is the most commonly reported subtype of PCNSL in dogs (14). Differential diagnoses such as reticulosis or histiocytic sarcoma, which may be considered based on the cytoplasm-rich neoplastic cells, were effectively excluded, because of the negative immunoreactivity for histiocytic-markers Iba-1 and Pax-5. Microgliomatosis cerebri, typically characterized by diffuse infiltration along white matter tracts or occasionally presenting in the meninges a as a non-mass-forming lesion (9), was ruled out due to lack of Iba-1 expression, a marker for microglial and histiocytic cells. An additional differential diagnosis, meningeal mastocytoma, was considered due to the presence of numerous slightly granulated, cytoplasm-rich tumor cells. However, toluidine blue staining failed to reveal metachromatic granules, thereby excluding this entity as well.

Conclusion

Due to limited CSF cell count, PCR-based clonality testing (PARR) was not possible. Despite the neurological examination and CSF analysis suggesting an intracranial process, MRI revealed no CNS abnormalities. Definitive evidence of PCNSL was found at postmortem examination, mainly through histopathology.

These findings highlight that accurate diagnosis and classification of neoplastic brain lesions require more than one diagnostic modality.

Unusual cases may go unrecognized when patients are euthanized at an early stage, often because owners face uncertain prognoses, limited diagnostic clarity, or the financial burden of advanced imaging and treatment.

This raises ethical questions:
From a scientific perspective, definitive diagnoses are invaluable, as outcomes and prognostic data for canine PCNSL are still extremely limited (8). Yet how far should diagnostic efforts go, particularly when animal welfare is weighed against cost and limited therapeutic success?
Even with a confirmed diagnosis, the prognosis for PCNSL is guarded, and reports of effective treatment are few (28).

To summarize, the presented case underscores the complexity of diagnosing PCNSL in dogs. To ensure the best possible diagnostic accuracy for the patient, a comprehensive multimodal approach and diagnostic strategy, integrating clinical findings, CSF analysis, and advanced imaging is recommended. The unusual immunohistochemical behavior in this case indicates the need for further research into the phenotypic diversity of PCNSL in dogs.
Finally, this case report invites a critical discussion about the ethical boundaries of diagnostics in veterinary medicine – balancing scientific gain and patient welfare.

6 References

1. Nirmal RM. Diagnosis of malignant lymphoma - An overview. J Oral Maxillofac Pathol. 2020;24(2):195–199.
2. Sisó S, Marco-Salazar P, Moore PF, Sturges BK, Vernau W, Wisner ER, et al. Canine Nervous System Lymphoma Subtypes Display Characteristic Neuroanatomical Patterns. Vet Pathol. 2017 Jan;54(1):53–60.
3. Villano JL, Koshy M, Shaikh H, Dolecek TA, McCarthy BJ. Age, gender, and racial differences in incidence and survival in primary CNS lymphoma. Br J Cancer. 2011 Oct;105(9):1414–1418.
4. Song RB, Vite CH, Bradley CW, Cross JR. Postmortem Evaluation of 435 Cases of Intracranial Neoplasia in Dogs and Relationship of Neoplasm with Breed, Age, and Body Weight. Vet Int Med. 2013 Sep;27(5):1143–1152.
5. Childress MO, Avery A, Behling-Kelly E, Bennett P, Brockley L, Dickinson R, et al. Diagnosis and Classification of Primary Nodal Lymphomas in Dogs: A Consensus of the Oncology-Pathology Working Group. Vet Comp Oncology. 2025 May 19;vco.13064.
6. Louis DN, Perry A, Wesseling P, Brat DJ, Cree IA, Figarella-Branger D, et al. The 2021 WHO Classification of Tumors of the Central Nervous System: a summary. Neuro-Oncology. 2021 Aug 2;23(8):1231–1251.
7. Summers BA, Cummings JF, Delahunta A. Veterinary neuropathology. St. Louis, Missouri: Mosby; 1995:351–381
8. Schmidt JM, Meichner K. Tumoren hämatopoetischer und lymphatischer Gewebe. In: Kessler M. Kleintieronkologie: Diagnose und Therapie von Tumorerkrankungen bei Hund und Katze. 4. vollständig überarbeitete Auflage. Stuttgart: Thieme Verlag; 2022:753-789
9. Cantile C, Youssef S. Neoplastic Diseases of the Nervous System. In: Jubb, Kennedy and Palmer’s Pathology of Domestic Animals, 6th edition, Philadelphia: Elsevier Health Sciences; 2015:403.
10. Forterre F, Davies F, Tumoren des Nervensystems. In: Kessler M. Kleintieronkologie: Diagnose und Therapie von Tumorerkrankungen bei Hund und Katze. 4., vollständig überarbeitete Auflage. Stuttgart: Thieme; 2022:709-719
11. Snyder JM, Shofer FS, Winkle TJV, Massicotte C. Canine Intracranial Primary Neoplasia: 173 Cases (1986–2003). J Vet Intern Med. 2006 May-Jun;20(3):669-675.

12. Dandachi D, Ostrom QT, Chong I, Serpa JA, Giordano TP, Kruchko C, et al. Primary central nervous system lymphoma in patients with and without HIV infection: a multicenter study and comparison with U.S national data. Cancer Causes Control. 2019 May;30(5):477–488.
13. Rissi DR, McHale BJ, Miller AD. Primary nervous system lymphoma in cats. J Vet Diagn Invest. 2022 Jul;34(4):712–717.
14. Fonti N, Parisi F, Aytaş Ç, Degl'Innocenti S, Cantile C. Neuropathology of Central and Peripheral Nervous System Lymphoma in Dogs and Cats: A Study of 92 Cases and Review of the Literature. Animals. 2023 Feb 27;13(5):862.
15. Song RB, Vite CH, Bradley CW, Cross JR. Postmortem Evaluation of 435 Cases of Intracranial Neoplasia in Dogs and Relationship of Neoplasm with Breed, Age, and Body Weight. Vet Int Med. 2013 Sep;27(5):1143–1152.
16. Zandvliet M. Canine lymphoma: a review. Veterinary Quarterly. 2016 Apr 2;36(2):76–104.
17. Couto CG. Lymphoma. In: Nelson RW, Couto CG, editors. Small animal internal medicine. Sixth edition. St. Louis, Missouri: Elsevier; 2020:1301.
18. Nielsen L, Thompson H, Hammond GJ, Chang Y, Ramsey IK. Central diabetes insipidus associated with primary focal B cell lymphoma in a dog. Vet Rec. 2008 Jan;162(4):124–5.
19. Vail DM, Hematopoietic Tumors. In: Ettinger SJ, Feldman EC, Côté E, Textbook of Veterinary Internal Medicine. Eighth edition. St Louis, Missouri: Elsevir; 2017:5000-5032.
20. Tamura S, Tamura Y, Nakamoto Y, Ozawa T, Uchida K. MR imaging of histiocytic sarcoma of the canine brain. Vet Radiol Ultrasound. 2009 Mar;50(2):178–181.
21. Hecht S, Adams WH. MRI of Brain Disease in Veterinary Patients Part 2: Acquired Brain Disorders. Vet Clin North Am Small Anim Pract. 2010 Jan;40(1):39–63.
22. Palus V, Volk HA, Lamb CR, Targett MP, Cherubini GB. MRI features of CNS lymphoma in dogs and cats. Vet Radiol Ultrasound. 2012 Jan;53(1):44–49.
23. Ródenas S, Pumarola M, Gaitero L, Zamora À, Añor S. Magnetic resonance imaging findings in 40 dogs with histologically confirmed intracranial tumours. Vet J. 2011 Jan;187(1):85–91.
24. Müller E, Klinische Mikrobiologie. In: Moritz A. Klinische Labordiagnostik in der Tiermedizin. 7., vollständig überarbeitete und erweiterte Auflage. Stuttgart: Schattauer GmbH; 2014:598.

25. Schwendenwein I, Moritz A. Quickfinder. In: Schwendenwein I, Moritz A, editor. LaborSkills. 3., aktualisierte Auflage. Stuttgart: Thieme; 2025:288
26. Ferreri AJM, et al. Primary central nervous system lymphoma. Nat Rev Dis Primers. 2023 Jun 15;9(1):29.
27. Bennett P, Williamson P, Taylor R. Review of Canine Lymphoma Treated with Chemotherapy - Outcomes and Prognostic Factors. Vet Sci. 2023 May11;10(5):342.
28. Mizutani Y, Inoue Y, Goda Y, Mizutani S, Asanuma T, Miura N, et al. Successful Treatment of Central Nervous System Lymphoma with Combination Therapy of Nimustine and Prednisolone in Two Dogs. Vet Sci. 2023 Aug 22;10(9):533.
29. Lampe R, Levitin HA, Hecht S, Vieson MD, Selting KA, Hague DW, et al. MRI of CNS lymphoma with choroid plexus involvement in five dogs and one cat. J Small Anim Pract. 2021 Aug;62(8):690–699.
30. Barajas RF, Politi LS, Anzalone N, Schöder H, Fox CP, Boxerman JL, et al. Consensus recommendations for MRI and PET imaging of primary central nervous system lymphoma: guideline statement from the International Primary CNS Lymphoma Collaborative Group (IPCG). Neuro-Oncology. 2021 Jul 1;23(7):1056–1071.
31. Schmidt MJ, Hoffmann M, Tipold A. Entzündliche Erkrankungen des Zentralnervensystems. In: Schmidt M, Kramer M. MRT-Atlas ZNS-Befunde bei Hund und Katze. Stuttgart: Enke Verlag; 2015:130-139.
32. Fuchs-Baumgartinger A, personal communication, Vetmeduni Vienna, May 2025